سال 93

Device Modeling of Nano-Structured Solar Cells

The first goal of our device modeling is to simulate the *J–V curve of a* nano-structured solar cell, both in dark and under illumination

1-Broad class of nano-structured solar cells

2-Describe the characteristics of the 'unit cell' on a microscopic scale

3-Two models will be presented to combine the multitude of unit cells to the macroscopic solar cells:

- 4-The network model (NM)
- 5-The effective medium model (EMM)

6- Both models are compared

7-Their results are presented and discussed

8-Finally, it is discussed how these models have to be adapted to include excitonic effects

By: Dr. Jabbari

Common Characteristics of Nano-Structured Solar Cells

consists of two phases

n-part or n-phase

conducts electrons

example, TiO_2 or a polymer derived from fullerene, C_{60}

In organic solar cells, the term acceptor material

p-part or p-phase

hole-conducting

for example, CuInS2 or a polymer derived from PPV, poly-phenyl-vinylene.

organic solar cells the term donor material

The core phenomena of the solar cell are taking place on a microscopic (even 'nano-scopic') scale at the boundary between the two constituent phases

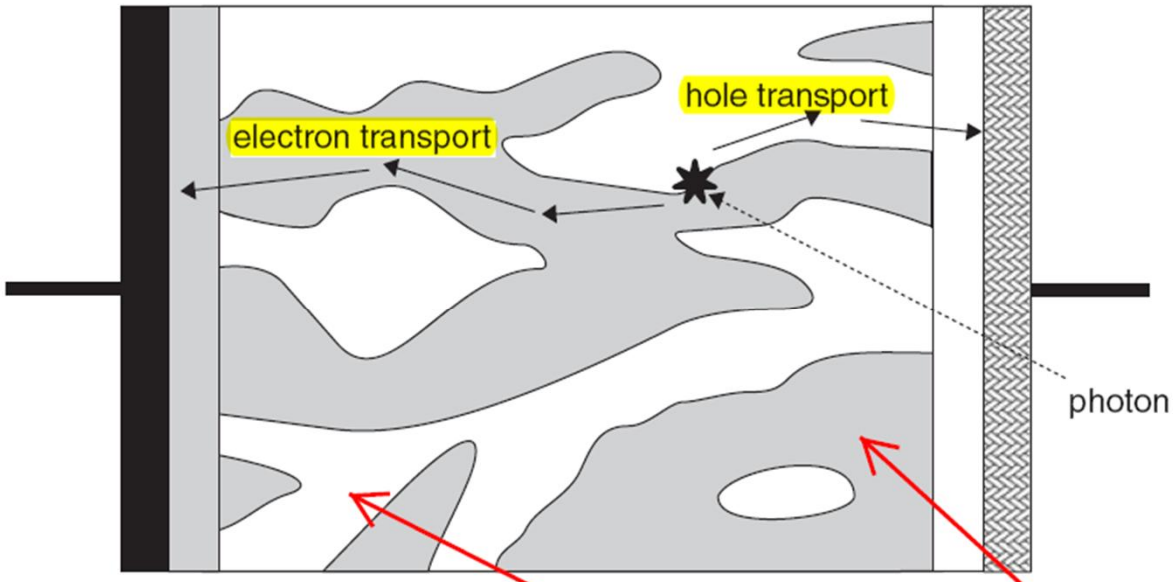

Fig. 1. An example of a nano-structured solar cell. The hatched phase is an electron transporting material, for example, the fullerene-derivate PCBM, and is only contacted by the left-hand-side electrode. The white phase is a hole-transporting material, for example, the PPV derivate MDMO-PPV, and is only contacted by the right-hand-side electrode. The phenomena of photon absorption, generation and separation of an electron and a hole, and transport of the carriers to the electrodes are shown schematically. The figure is not to scale: the width of the white and hatched channels is typically 1–50 nm, and the total cell width is 0.1–10 μm.

We call the microscopic environment, where these phenomena take place, the *elementary cell or unit cell*. *Often, a macroscopic* solar cell is an assembly of a multitude of almost identical elementary cells; this assembly is in the form of two interpenetrating networks

2.2. Classification of Nano-Structured Solar Cells

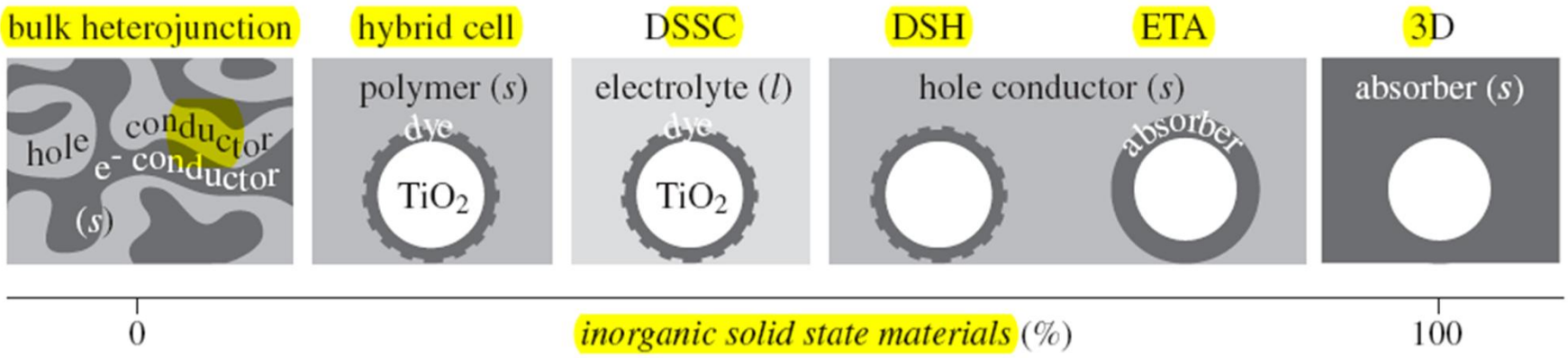

Fig. 2. Schematic representation of nano-structured solar-cell examples on unit cell scale: from an all organic cell to an all inorganic solid-state cell; the various cell types are described in the text.

The 100% organic nano-structured cell is a mixture

In a 'bulk heterojunction' cell

- polymer/polymer blend (e.g., MDMOPPV/ PCNEPV [2])
- or a polymer/organic molecule blend (e.g., MDMO-PPV/PCBM and 6,6-phenyl C61-butyric acid methyl ester (PCBM)

blends of poly 2-methoxy-5-3, 7-dimethyloctyloxy-1,4-phenylene vinylene (MDMO-PPV) and poly-oxa-1,4-phenylene-1-cyano-1,2-vinylene-2-methoxy-5-3, 7-dimethyloctyloxy-1,4-phenylene-1,2-2-

مقدار کمی از ساختارهای ارگانیک و مختلط در قسمت n-type خود از شبکه متخلخل نانو استفاده می کنند
به عنوان مثال در TiO2 تنها حدود 20 تا 100 نانو متر استفاده می شود

In case the absorber is a monomolecular layer of an organic dye, and the hole conductor a liquid electrolyte, the cells are called dye-sensitized solar cells (DSSCs) or Grätzel cells

the liquid electrolyte by an organic solid hole conductor like OMeTAD or a polymer

When the electrolyte replacing material is an inorganic solid-state hole conductor like CuSCN [7] or CuI [8], the cells are called dye sensitized ***heterojunctions*** (DSHs), or interpenetrating heterojunctions (i-hets).

If solid-state absorber is CdTe , a-Si or CuInS2 the cells thus obtained are the so-called *extremely thin absorber (ETA)* cells

THE CONCEPT OF THE FLAT-BAND SOLAR CELL

At these lines, Neumann-type boundary conditions apply for the electrostatic potential ϕ *that* $\partial\phi/\partial x = 0$ *and no* current crosses these lines in the *x-direction*

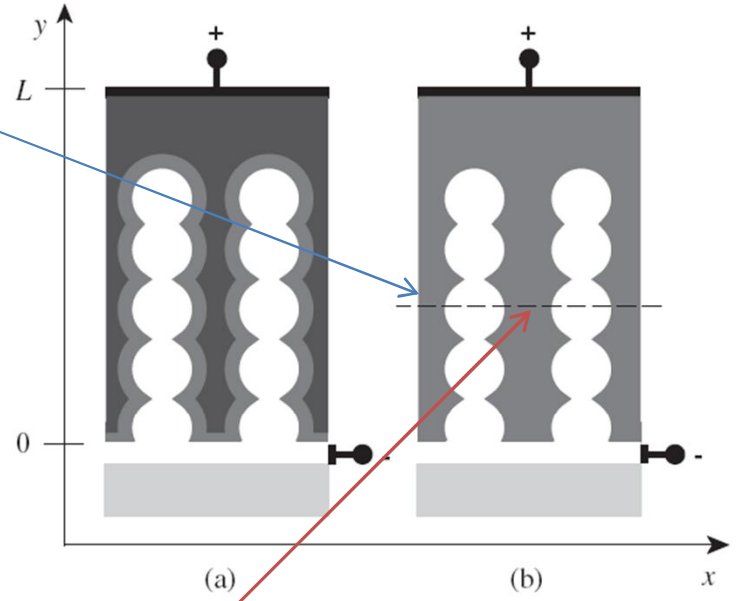

Fig. 3. Simplification of the geometry of the nano-structured solar cell of Fig. 1 into columns of grains; structure of a DSSC. (a) Each column is contacted by a well-conducting electrolyte; structure of a solid-state 3-Dcell (or ETA-cell in which the absorbing material is absorber and hole conductor in one), (b) Each column is contacted by a conducting solid-state material; at the dashed line there is a periodic ordering of TiO_2/absorber.

In order to start the device modeling we simplify the geometric ordering of Fig. 1.

In a Grätzel type cell, a well-conducting electrolyte, almost perfectly, contacts all individual TiO2/dye grains

the structure of Fig. 3(a) is obtained

For solid-state TiO2-based cells (eta-cells, 3-D cells), the arrangement of Fig. 3(b) is more appropriate, as there is no separate hole conductor penetrating into the structure.

Along the dashed line a periodic, nano-scale ordering: either of *n-type TiO2 grains* and their *p-type absorber shell (eta-cells, 3-D cells), or of the n- and p-type* constituents of an organic bulk heterojunction solar cell.

polymer bulk heterojunctions also can be simplified to the structure of Fig. 3(b)

A Solar Cell with Periodic Boundary Conditions

the dashed line in Fig. 3 is further simplified in Fig. 4.

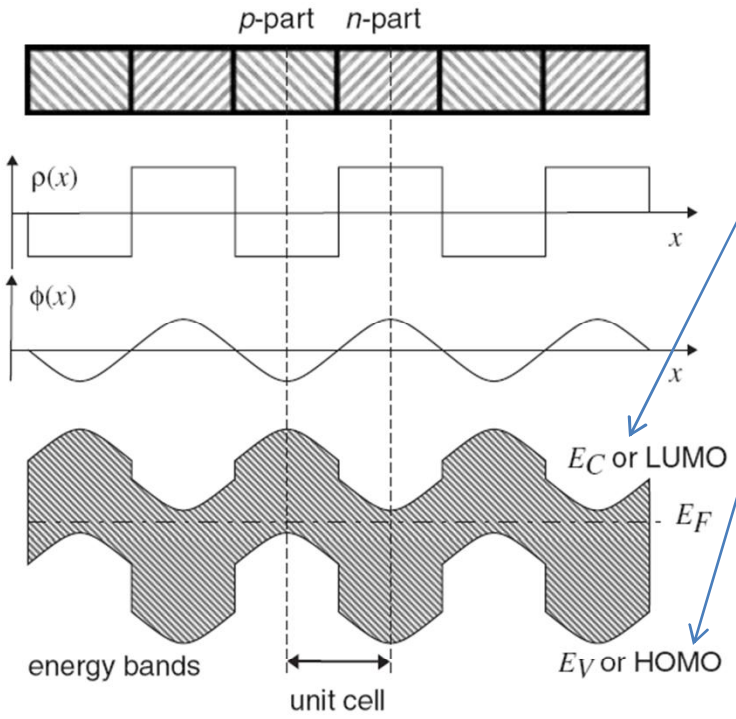

$$E_C(x) = -q\phi(x) - \chi(x)$$

$$E_V(x) = -q\phi(x) - \chi(x) - E_g(x)$$

where χ is the electron affinity

در شیمی و فیزیک اتمی **میل ترکیبی الکترون** (به انگلیسی: Electron affinity) یک اتم یا مولکول به معنای انرژی است که هنگام اضافه شدن یک الکترون به یک اتم یا مولکول خنثی آزاد و تبدیل آن به یک یون منفی (آنیون) ایجاد می‌شود.

X + e− → X− + energy (انرژی)

در فیزیک حالت جامد میل ترکیبی الکترون معنای گوناگونی دارد و به معنای انرژی به دست آمده از حرکت یک الکترون از فضای خلاء در خارج از نیمه هادی به سمت پایین باند هدایت درون نیمه هادی است.

Fig. 4. A periodic ordering of *n*-type TiO_2 and a *p*-type absorber. The charge density $\rho(x)$, the electrostatic potential $\phi(x)$ and the equilibrium band diagram are sketched. The hatched region in the band diagram is the energy gap. A unit cell with periodic boundary conditions is indicated. Reprinted with permission from J. Appl. Phys., Vol. 95–94, M. Burgelman and C. Grasso, A network of flat-band solar cells as a model for solid-state nano-structured solar cells, pp. 2020–2024 ©2004, American Institute of Physics

میل ترکیبی الکترون تنها در حالت گاز ی ماده تعریف شده است. به این دلیل که سطح انرژی مولکول‌ها و اتم‌ها در حالات مایع و جامد به دلیل پیوندها میان اتمی و مولکولی ویژه در این حالات، تحت تاثیر مولکول‌ها و اتم‌های مجاور خویش قرار می‌گیرد

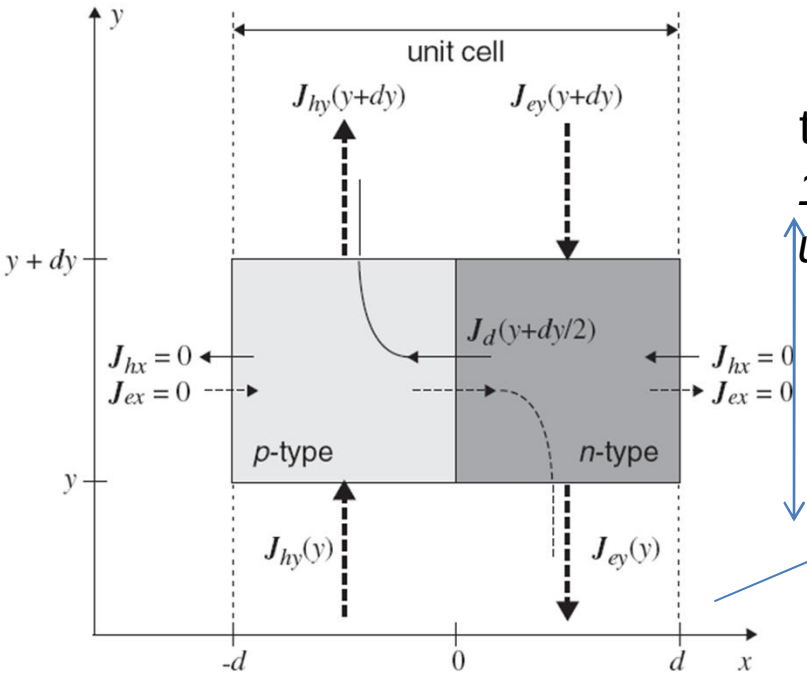

the total cell thickness *L* *is 100 nm for a polymer cell and up to 10m for* a DSSC

the dimension *d of the unit cell is a few nanometer for* a polymer cell to a few tens of a nanometer for a TiO2-based cell,

Fig. 5. A unit cell in a nano-structured solar cell under current-carrying conditions. J_e and J_h are the electron and hole particle currents. A lateral current (in x-direction) J_d is generated through the junction of the unit cell diode at $x = 0$, but $J_{ex} = J_{hx} = 0$ at the borders of the unit cell ($x = -d$ and $+d$). The hole current J_{hy} is collected at the top ($y = L$) of the p-type subnetwork, and the electron current J_{ey} is collected at the bottom ($y = 0$) of the n-type subnetwork.

We will thus treat our unit cell as if there were no *y-variations*

(thus as a 1-D cell)

The Unit Cell is a Flat-Band Solar Cell

- The first step is calculating the *J–V* characteristics of a single unit cell
- *This is difficult to handle analytically:* because, due to the small dimensions, the usual photovoltaic cell concepts do not apply (e.g., the concept of depletion layer, quasi-neutral region, diffusion of minority carriers, etc.).
- Also a numerical calculation is problematic for most common photovoltaic device simulators, including SCAPS [17, 18] and PC-1D [19], as no Neumann-type boundary conditions are implemented

an easy approximation based on the fact that there is almost no electrostatic potential drop over the unit cell: the unit cell is in essence a 'flat-band cell'

سال ۹۳

$$\Delta\phi = \frac{2Nd^2}{2\varepsilon_s \varepsilon_0}$$

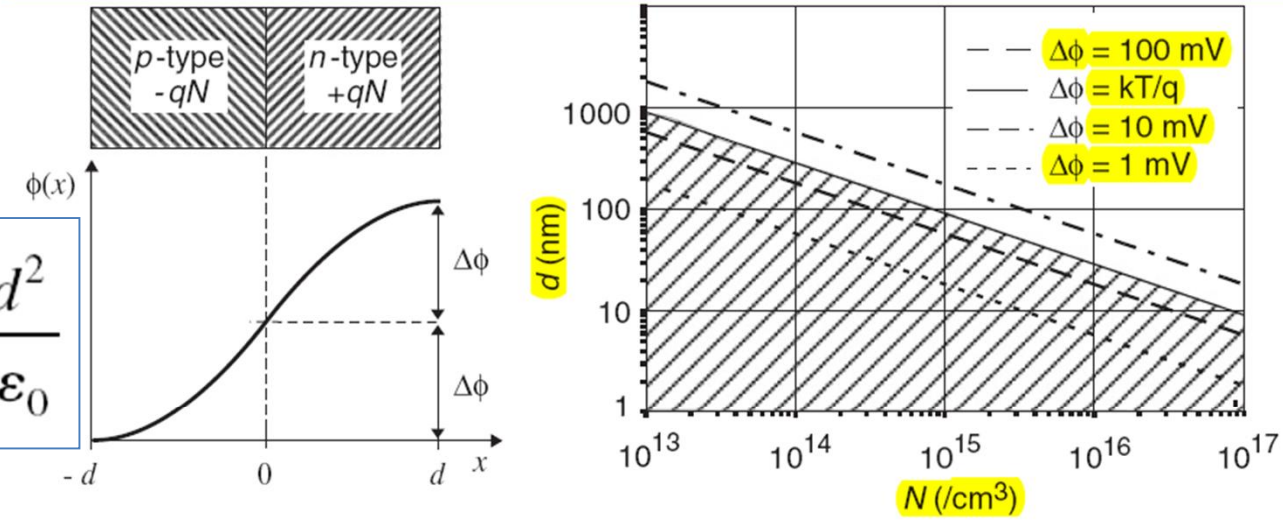

Fig. 6. Left-hand side: A unit cell with periodic boundary conditions ($\partial\phi/\partial x = 0$ at $x = \pm d$) and an electrostatic potential drop $\Delta\phi$ over each side. The p-side ($-d < x < 0$) carries a charge density $-qN$, and the n-side ($0 < x < d$) a charge density $+qN$. Right-hand side: The thickness/carrier density combinations (N,d) for a given potential drop $\Delta\phi$, calculated with Eq. (2) and $\varepsilon_s = 3$. All cells in the hatched region to the left-hand side and below the line $\Delta\phi = kT/q$ can be considered as flat-band solar cells.

This argument is now validated by numerical calculations of a CdTe/TiO2 eta-cell with the device simulator SCAPS [17, 18]. As all other common solar cell simulation tools available, SCAPS can only handle Dirichlet type boundary (till 2007)

The kink at *x=0 is caused by the large* difference in dielectric constant between TiO2 *(4) and CdTe (10).*

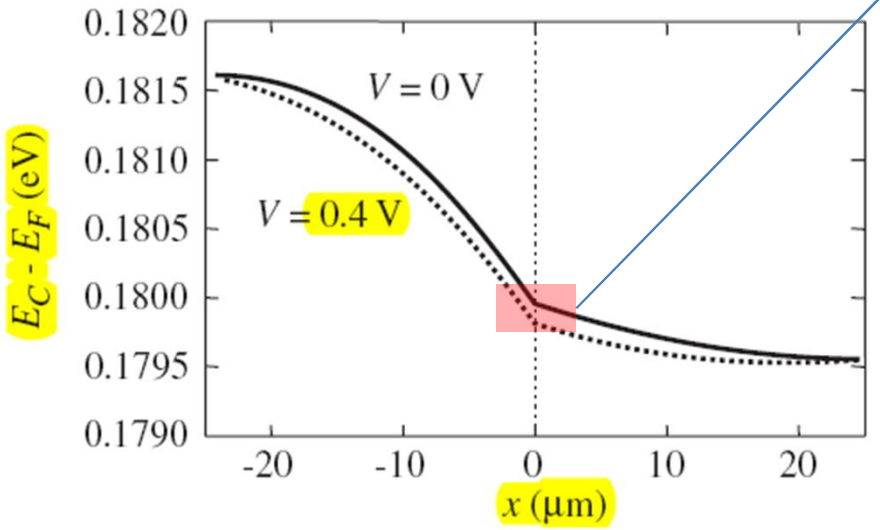

Fig. 7. SCAPS simulation of the electrostatic potential $\phi(x)$ of a thin $CdTe/TiO_2$ nano-structured unit cell. Solid curve: zero bias $V = 0$; dotted curve: forward bias ($V = 0.4$ V). To mimic the Neumann boundary conditions ($\partial\phi/\partial x = 0$ at the boundaries), specific values for the 'contact work function' are used: $\Phi^{TiO_2} = 4.6796$ eV and $\Phi^{CdTe} = 4.6816$ eV (at zero bias) or 5.0816 eV (at 0.4 V bias). Reprinted with permission from J. Appl. Phys., Vol. 95–94, M. Burgelman and C. Grasso, A network of flat-band solar cells as a model for solid-state nano-structured solar cells, pp. 2020–2024 ©2004, American Institute of Physics.

The Flat-Band Solar Cell: Energy Band Diagram

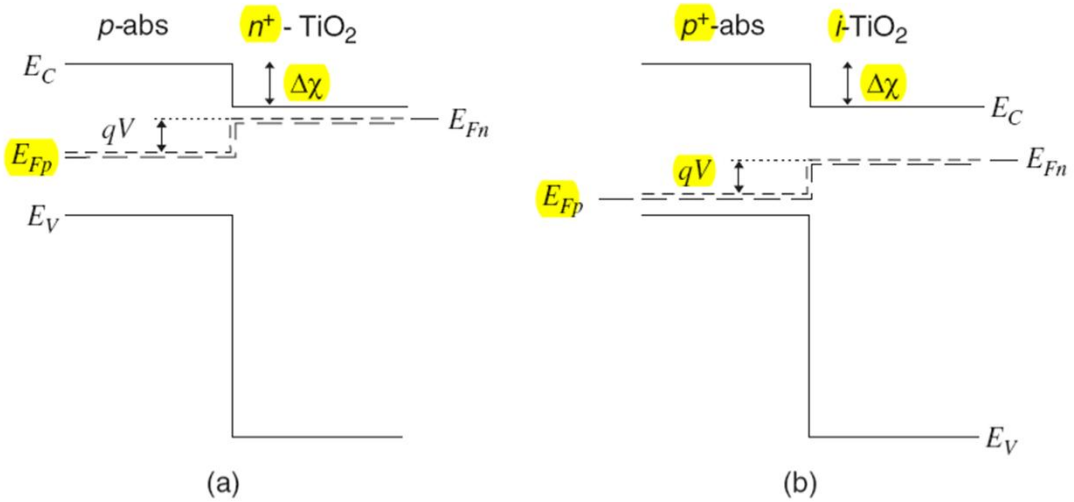

current is driven by a separation *qVd between the Fermi levels*, where *Vd is by definition the 'applied voltage' over the unit cell*

Fig. 8. Flat-band approximation of a unit cell in a periodic structure. (a) In case the *n*-region is doped more heavily. (b) In case the *p*-region is doped more heavily.

even higher values of $\Delta\chi$, up to 0.7 eV were reported

For TiO2 ➔*Eg>3 eV*

for p-absorbers used in eta and 3-D cells, for example, CuInS2 or CdTe, this is not so strongly justified since *Eg is only1.5 eV.*

In organic photovoltaic materials including most polymers and fullerenes,

$$E_{Fn}(\mathrm{TiO_2}) - E_{Fp}(\mathrm{absorber}) = qV_d$$

most simple case

$(d^{\mathrm{TiO_2}} = d^{\mathrm{abs}})$

effective density of states

$$N_V^{\mathrm{TiO_2}} = N_C^{\mathrm{TiO_2}} = N_V^{\mathrm{abs}} = N_C^{\mathrm{abs}}$$

In a pn^+ cell with $N_D^{\mathrm{TiO_2}} \gg N_A^{\mathrm{ab}}$

$$N_A^{\mathrm{abs}} + n^{\mathrm{abs}} - p^{\mathrm{abs}} = N_D^{\mathrm{TiO_2}} - n^{\mathrm{TiO_2}} + p^{\mathrm{TiO_2}}$$

$$N_A^{\mathrm{abs}} \approx N_D^{\mathrm{TiO_2}} - n^{\mathrm{TiO_2}}$$

$$E_C(\mathrm{TiO_2}) - E_{Fn}(\mathrm{TiO_2}) = kT \ln\left(\frac{N_C^{\mathrm{TiO_2}}}{N_D^{\mathrm{TiO_2}} - N_A^{\mathrm{abs}}}\right)$$

At high forward bias V, E_{Fp} *approaches the* valence band in the absorber, and holes become important (Fig. 9).

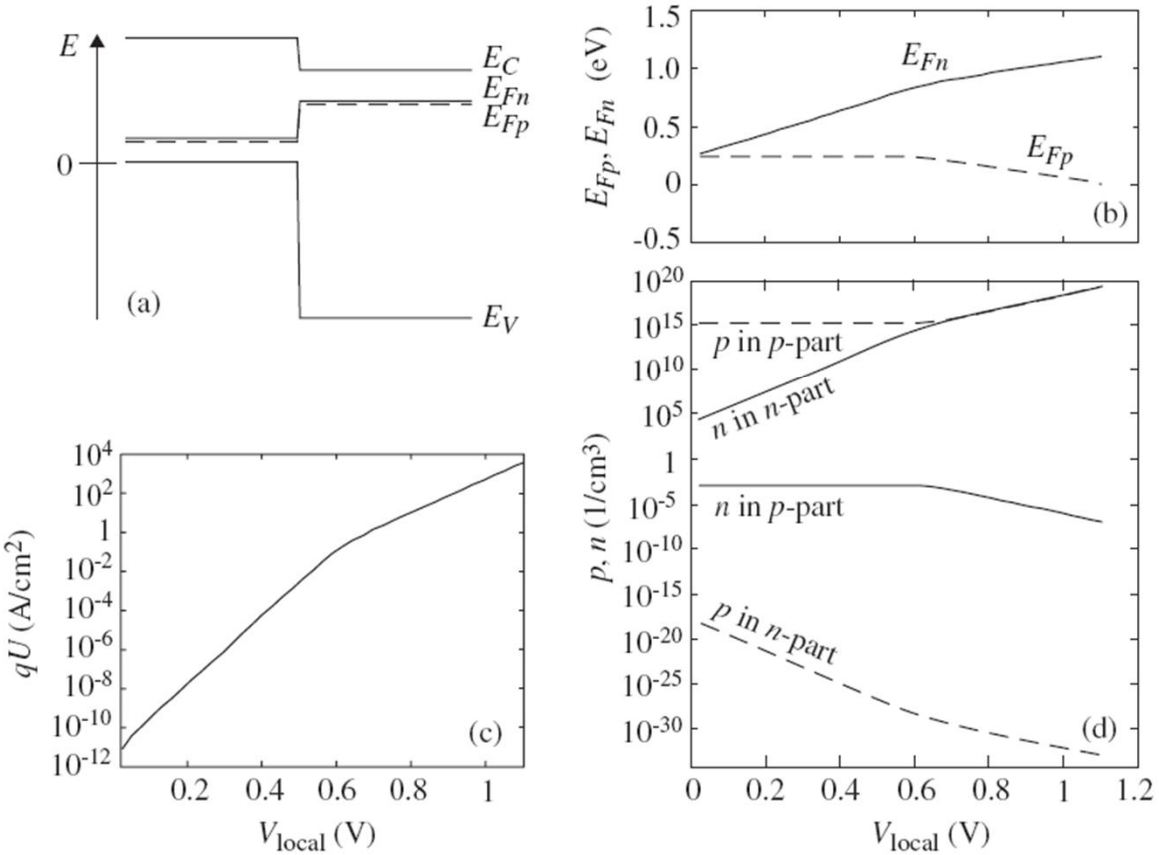

Fig. 9. Analysis of a flat-band p^+-absorber/n-TiO_2 solar cell. (a) Upper left-hand side: band diagram at $V_{local} = 0.5$ V with definition of energies, (b) Upper right-hand side: position of the Fermi levels $E_{Fp}(V_{local})$ and $E_{Fn}(V_{local})$, (c) Lower left-hand side: dark diode current $qU(V_{local})$, (d) Lower right-hand side: carrier concentrations $n(V_{local})$ and $p(V_{local})$. Parameter values: p-side: $N_A = 10^{15}\,cm^{-3}$ and $E_g = 1.5$ eV; n-side: $N_D = 10^{10}\,cm^{-3}$ and $E_g = 3$ eV; both sides $d = 25$ nm; junction: $\Delta\chi = 0.4$ eV; $\tau = 1$ ns; $S_i = 5\ 10^3$ cm/s.

By: Dr. Jabbari

In a p^+n cell (with $N_A^{abs} \gg N_D^{TiO_2}$; Fig. 8(b)

$N_D^{TiO_2} \to 0$), electrons in the absorber can be neglected,

$$N_A^{abs} + n^{abs} - p^{abs} = N_D^{TiO_2} - n^{TiO_2} + p^{TiO_2}$$

$$N_A^{abs} - p^{abs} \approx 0$$

$$E_{Fp}(\text{abs}) - E_V(\text{abs}) = kT \ln\left(\frac{N_V^{abs}}{N_A^{abs}}\right)$$

Fig. 9.

3.5. The Flat-Band Solar Cell: *J–V* Characteristics of the Unit Cell

The dark current Jd in flat-band solar cells is determined by recombination

Under low injection ⇒ recombination ⇒ excess minority carrier density (the equilibrium concentration

is only important in the absorber material

in a pn^+ cell ⇒ Fig. 8(a)), $n_{minor} = p^{abs}$

in a p^+n cell (Fig. 8(b)), $n_{minor} = n^{abs}$

$n_{minor} = n^{TiO_2}$

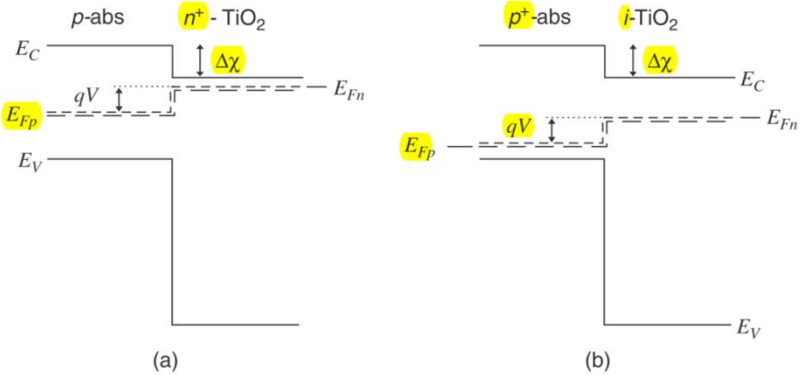

In all cases, n_{minor} varies exponentially with applied voltage V_d (Fig. 9),

recombination current

$$J_d = \frac{qd_p}{\tau}[n_{minor}(V) - n_{eq}]$$ bulk recombination, or

$$J_d = qS_i[n_{minor}(V) - n_{eq}]$$ interface recombination, with

$$n_{minor}(V) = n_{eq}\exp\left(\frac{qV}{kT}\right)$$

lifetime

interface recombination velocity

is the equilibrium minority concentration at the interface

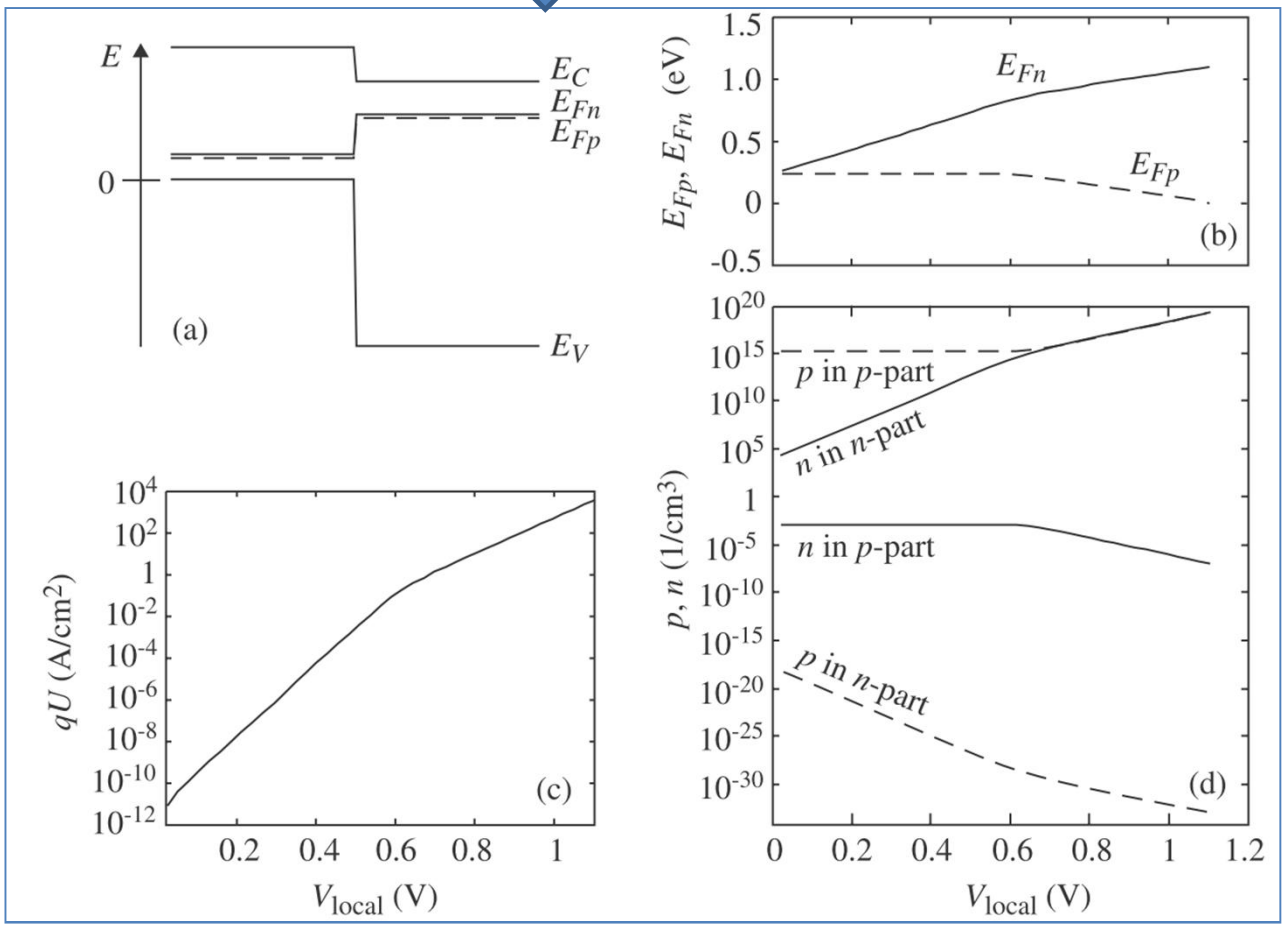
E
E_C
E_{Fn}
E_{Fp}
0
(a)
E_V
1.5
1.0
0.5
0
-0.5
E_{Fp}, E_{Fn} (eV)
E_{Fn}
E_{Fp}
(b)
10^{20}
10^{15}
10^{10}
10^{5}
1
10^{-5}
10^{-10}
10^{-15}
10^{-20}
10^{-25}
10^{-30}
p, n (1/cm³)
p in p-part
n in n-part
n in p-part
p in n-part
(d)
0 0.2 0.4 0.6 0.8 1 1.2
V_{local} (V)
10^{4}
10^{2}
1
10^{-2}
10^{-4}
10^{-6}
10^{-8}
10^{-10}
10^{-12}
qU (A/cm²)
(c)
0.2 0.4 0.6 0.8 1
V_{local} (V)

THE NETWORK MODEL (NM)

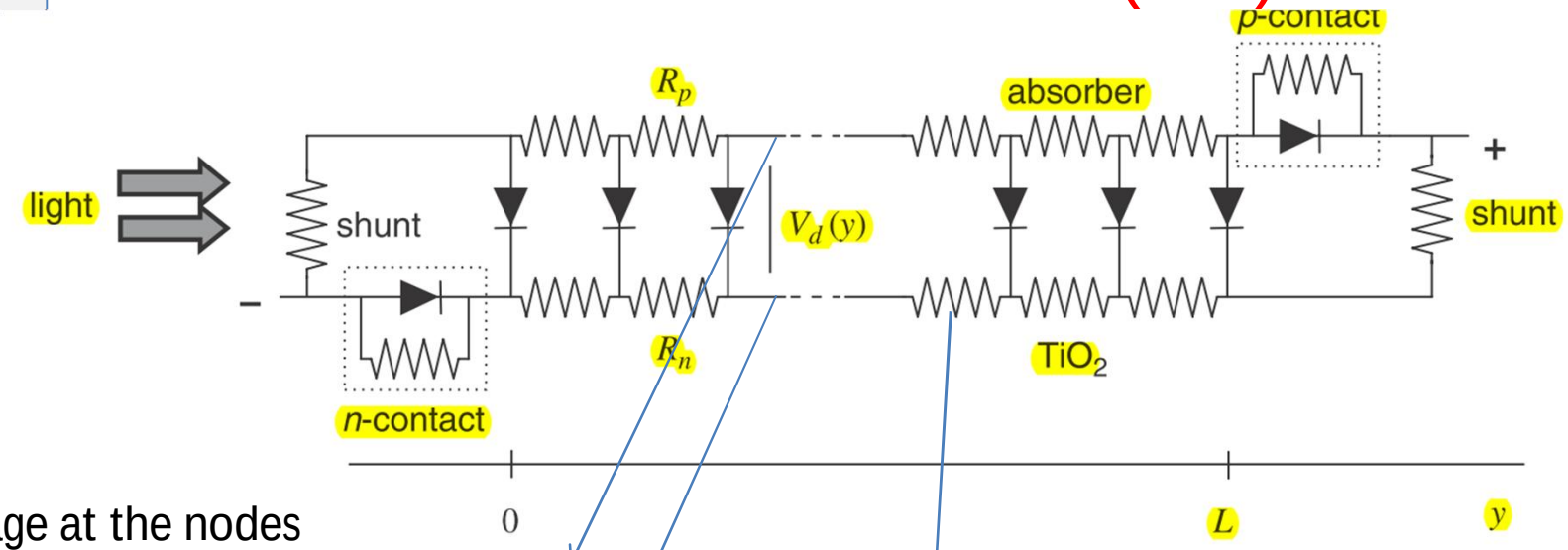

voltage at the nodes

represents the hole Fermi level E_{Fp} in the p-part of the unit cells

level E_{Fn} in the n-part of the unit cells

representation stand for transport by drift and diffusion

$$V_d(y) = \frac{1}{q}(E_{Fn}^{TiO_2} - E_{Fp}^{abs})\Big|_{\text{unit cell at position } y}$$

THE EFFECTIVE MEDIUM MODEL (EMM)

Another way to describe the macroscopic cell structure of a nano-structured solar cell

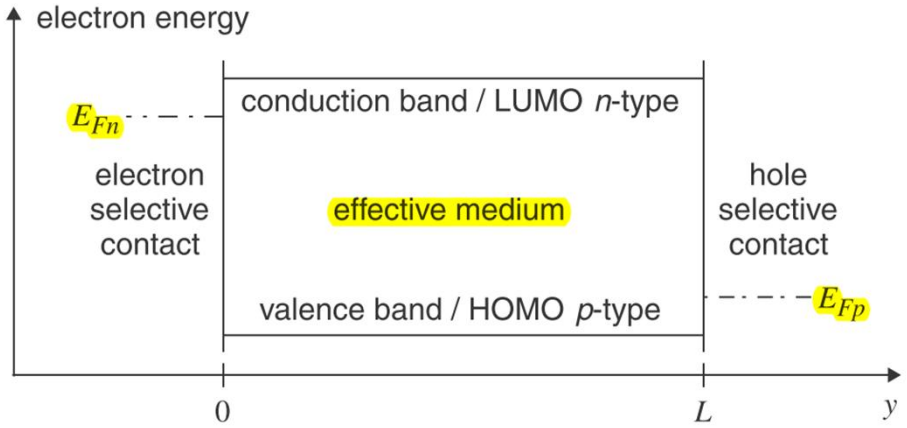

Fig. 11. In the EMM, the whole *p–n* nano-structure is represented by one single EM semiconductor layer. The EM has one conduction band namely the conduction band or LUMO of the *n*-type material and one valence band namely the valence band or HOMO of the *p*-type material. E_{Fn} and E_{Fp} represent the Fermi levels, respectively, of the electron and hole selective contact. For simplicity, the cell is shown in a flat-band condition.

This can be a dye/electrolyte combination in DSSC cells, an inorganic semiconductor in eta cells or 3-D cells, or a PPV derivate such as MDMO- PPV or MEH-PPV in a polymer/fullerene bulk heterojunction

To calculate the external J–V characteristics of the effective medium cell of Fig. 11, it is easiest to feed all parameters into a standard solar-cell device simulator, for example, SCAPS [16]. In this way it is also possible to define several EM layers in the cell structure, or even to define a grading of the materials parameters of the EM in the y-direction of the cell structure.

EXCITONIC SOLAR CELLS

فرآیندهای جذب اپتیکی

فرآیند1 در شکل مربوط به گذارهای الکترون (یا حفره) درون یک نوار، در نتیجه جذب انرژی فوتونی می‌باشد. نموداری از این گذارهای درون نواری ((intraband transitionsدر شکل(((bو ((3(aنشان داده شده است. این نوع گذار در فلزات و نیمه‌رساناهایی که تراکم حامل‌ها در یک نوار، قابل ملاحظه باشد از اهمیت برخوردار است.

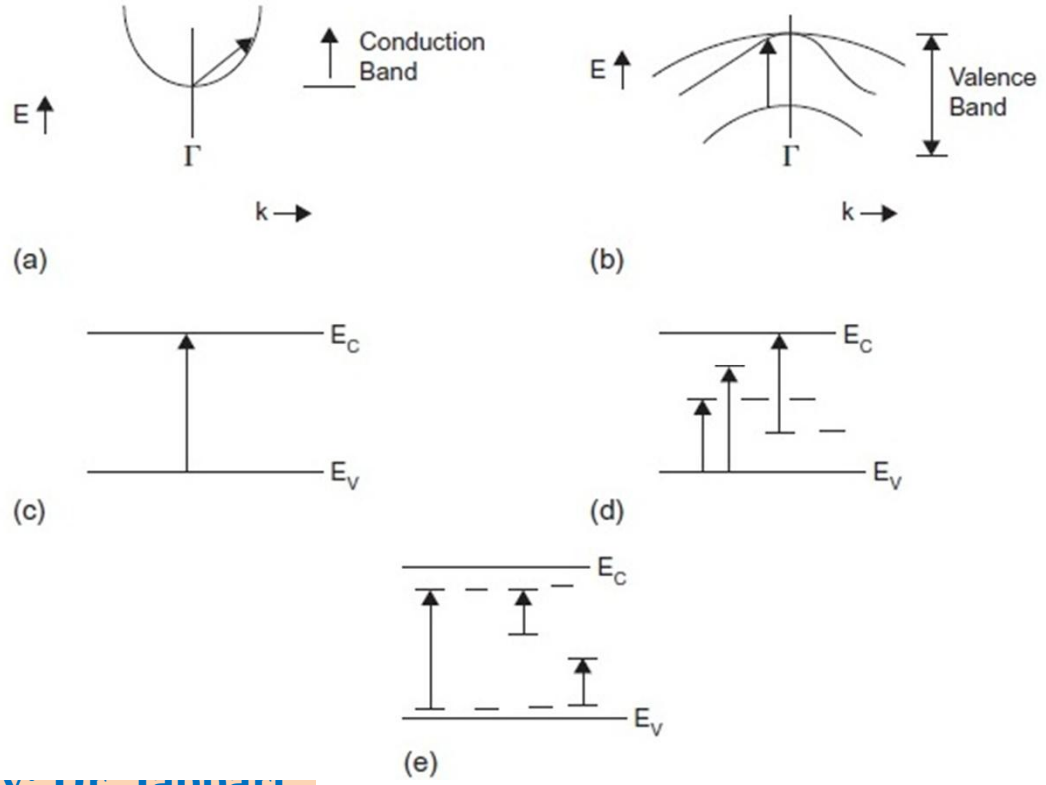

فرآیند2 در شکل(2) مربوط به جذب فونونی است؛ بدین معنی که نور با برانگیختن مدهای فونونی در ماده جذب می‌شود. الکترون‌ها در این فرآیند درگیر نمی‌شوند. به دلیل انرژی‌های کمی که فونون‌ها دارند، این فرآیند جذب در محدوده فروسرخ طیف نور رخ می‌دهد. فرآیند3 همه انواع گذار ناشی از جذب فوتون، بین ترازهای موجود در گاف نواری و همچنین بین ترازهای موجود در گاف و یک نوار را شامل می‌شود (شکل(((eو () (3(dترازهای انرژی در گاف نواری نیمه‌رسانا می‌تواند به دلیل وجود ناخالصی‌ها در نیمه‌رسانا بوجود آید. به این ترازهای انرژی الکترونی، حالت‌های جایگزیده ناشی از اتم‌های دهنده یا پذیرنده می‌گویند **فرآیند4 مربوط به جذب فوتون همراه با تولید اکسایتون‌ها (جفت‌های الکترون- حفره مقید ( )** exciton)است. **جذب در مواد ارگانیک، از قبیل مولکول‌های کوچک رنگ‌ها در سلول‌های خورشیدی رنگدانه‌ای (**dye-sensitized solar cells)**و جاذب‌های پلیمری در سلول‌های خورشیدی ارگانیک، عموماً یک فرآیند اکسایتونی است. همچنین در نانوذرات، اکسایتون‌ها نقش کلیدی در جذب دارند** .

Most often, the charge separation only takes place at the boundary between two organic phases (molecules or polymers) driven by favorable energetic conditions.

Electrons,→ e
holes→ h
Excitons→ x

total optical absorption $G(\lambda,y) = \Phi_0 \alpha(\lambda) \exp[-y\alpha(\lambda)]$

fraction f_{eh} of the absorbed light serves to generate electron–hole pairs.

fraction f_x to generate a bound exciton pair.

$$g_{eh}(\lambda,y) = f_{eh}(\lambda)G(\lambda,y) \quad \text{and}$$
$$g_x(\lambda,y) = f_x(\lambda)G(\lambda,y) \quad \text{with} \quad f_{eh}(\lambda) + f_x(\lambda) = 1$$

In inorganic semiconductors, $f_x \cong 0$.

In organic materials, $f_x \cong 1$ for all absorbed

Simple Exciton Model and Extensions

$$U_x = \frac{1}{\tau_x}(n_x - n_{x0})$$

where τ_x is the exciton lifetime.

Excitons also can dissociate and convert to a free electron–hole pair, with a net conversion rate $C_{x/eh}$

$$C_{x/eh} = b(n^* n_x - n_e n_h)$$

where b (in $cm^3 s^{-1}$) describes the strength of the exciton binding and n^* is an appropriate constant, with the dimension of concentration (thus in cm^{-3}).

In equilibrium to be zero

$$n_{x0} = n_i^2/n^*; \qquad J_x = -D_x \frac{dn_x}{dx}$$

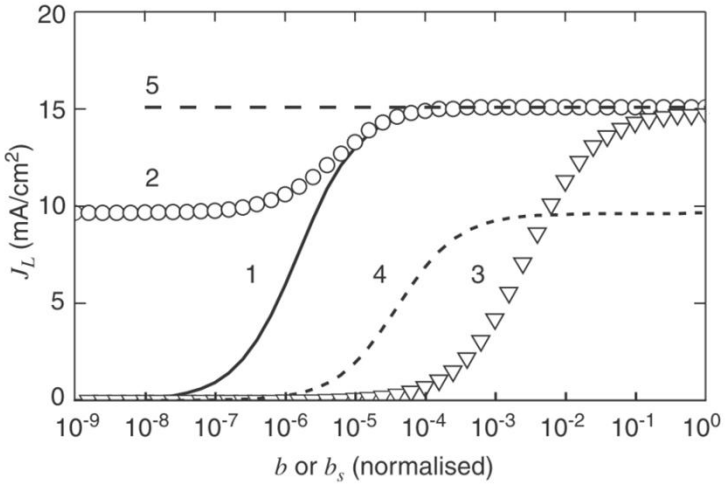

Fig. 18. Short-circuit current under uniform illumination ($\alpha \rightarrow 0$), generating excitons only ($f_x = 1$), for varying exciton dissociation parameters: surface dissociation at contact b_s: low = 10^{-2}/cms^{-1}, high = 10^{7}/cms^{-1}; bulk dissociation b: low = 10^{-16}/cm^{3}s^{-1}, high = 10^{-7}/cm^{3}s^{-1}; field-enhanced dissociation $b(E)$ in SCL: $b = b_{low}$ for $y > 0$ and exponentially increasing toward junction ($y = -W$). Curve (1): b varying and b_s = low. Curve (2): b varying and b_s = high. Curve (3): $b(E)$ varying and b_s = low. Curve (4): b_s varying and b = low. Curve (5): b_s varying and b = high. The horizontal axis is normalized to the high value of the varying parameter. Other parameters are: $L_e = L_x = x_0 = 50\,\mu$m and $S_e = S_x = 0$. Reprinted with permission from Thin Solid Films, Vol. 511–512, M. Burgelman and B. Minnaert, Including excitons in semiconductor solar cell modelling, pp. 214–218 © 2006, Elsevier.

CONCLUSION

Modeling of nano-structured solar cells is complicated for at least three features:

(i) The geometry of the nano-structure, be it a structure based on TiO2 nano-particles or a bulk heterojunction of organic materials, is very compli-cated and deviates far from the planar structure of bulk crystalline and even of polycrystalline thin film cells.

(ii) The distance scale at which the essential phenomena take place is very small: the typical distance is well below a m for an eta-cell, down to a few nm for an organic solar cell. This makes the application of nearly all concepts of the classical diode theory doubtful or even invalid.

(iii) In organic solar cells, molecular processes of excitation,injection, charge transfer and recombination exceed the framework of solid-state semiconductor physics. Owing to these three features, the straightfor-ward application of simulation programs available to the photovoltaic research community is rendered impossible.

AMPS

Analysis of Microelectronic and Photonic Structures

one-dimensional

numerically solves the three governing semiconductor device equations (the Poisson equation and the electron and hole continuity equations) without making any a-priori assumptions about the mechanisms controlling transport in these devices.

homojunction and heterojunction p-n and p-i-n, solar cells and detectors;

- homojunction and heterojunction p-n, p-i-n, n-i-n, and p-i-p microelectronic structures;
- multi-junction solar cell structures;
- multi-junction microelectronic structures;
- compositionally-graded detector and solar cell structures;
- compositionally-graded microelectronic structures;
- novel device microelectronic, photovoltaic, and opto-electronic structures;
- Schottky barrier devices with optional back layers.

output such as current voltage characteristics in the dark function of temperature.

collection efficiencies as a function of voltage, light bias, and temperature

electric field distributions, free and trapped carrier populations, recombination profiles, and individual carrier current densities as a function of position

Examples

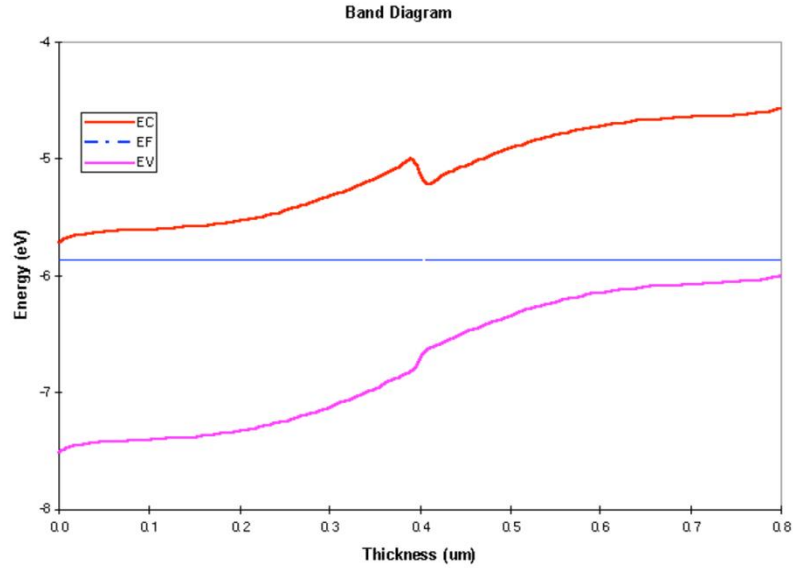

Figure1-2 Band structure in thermodynamic equilibrium.

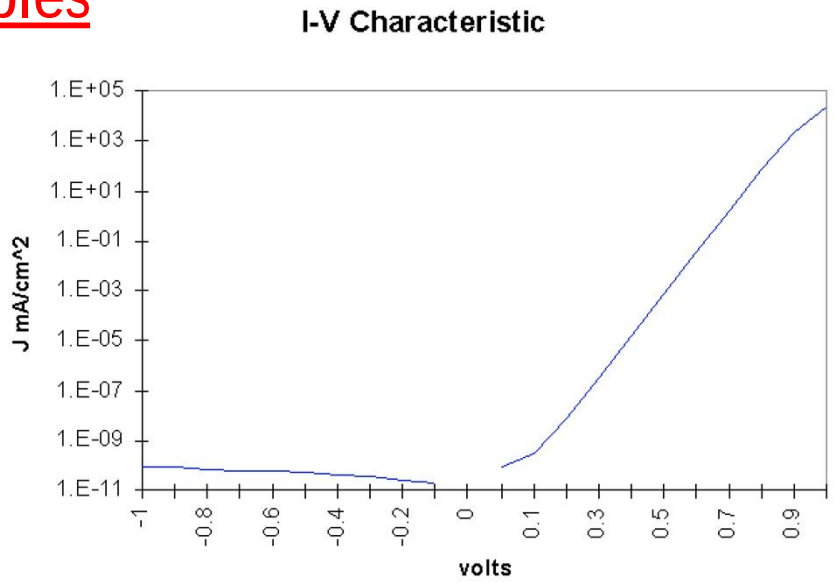

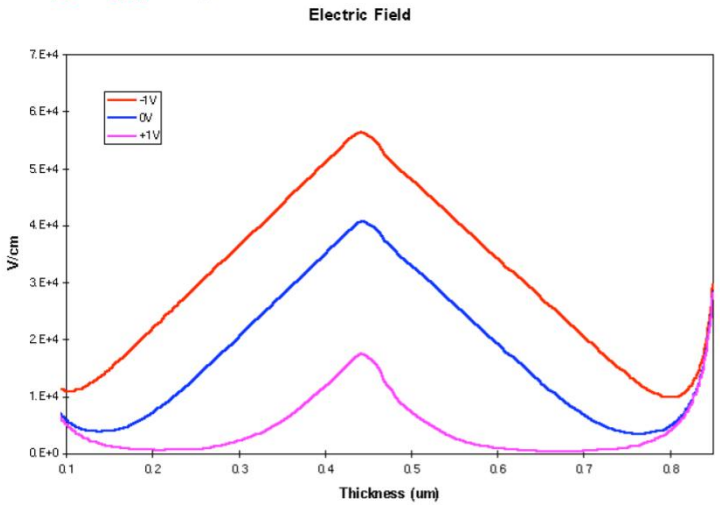

Figure 1-3 Spatial dependence of the electric field at three different bias voltages. -1V, 0V, 1V.

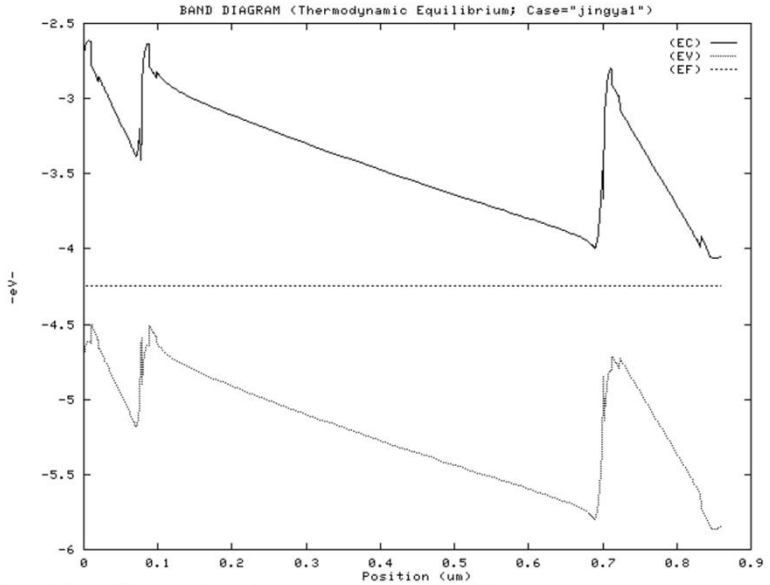

Figure 1-5. Band diagram of this triple junction in thermodynamic equilibrium.

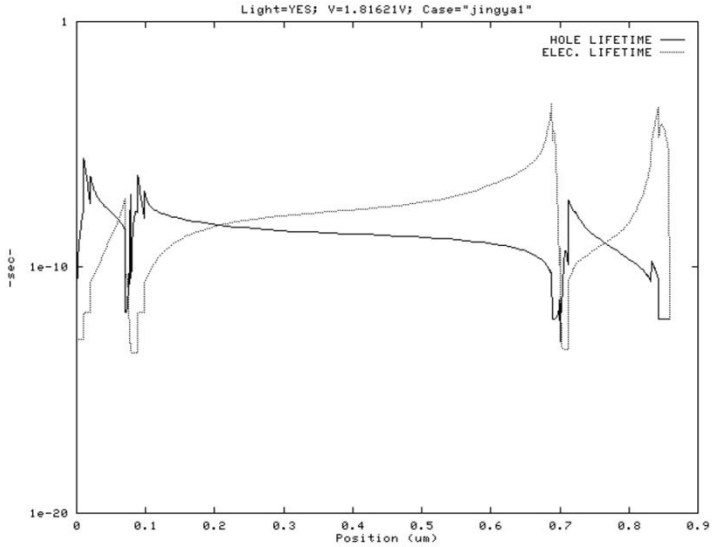

Figure 1-6. Electron and hole lifetime at V_{OC} versus position for a triple. Only meaningful for regions where carrier is the minority carrier.

MATHEMATICAL MODELING & SOLUTION TECHNIQUES

Poisson's Equation

$$\frac{d}{dx}\left(-\varepsilon(x)\frac{d\Psi'}{dx}\right) = q\cdot[p(x)-n(x)+N_D^{+}(x)-N_A^{-}(x)+p_t(x)-n_t(x)]$$

AMPS needs expressions for the six new dependent variables n, p, n_t, p_t, N_D+, and N_A-

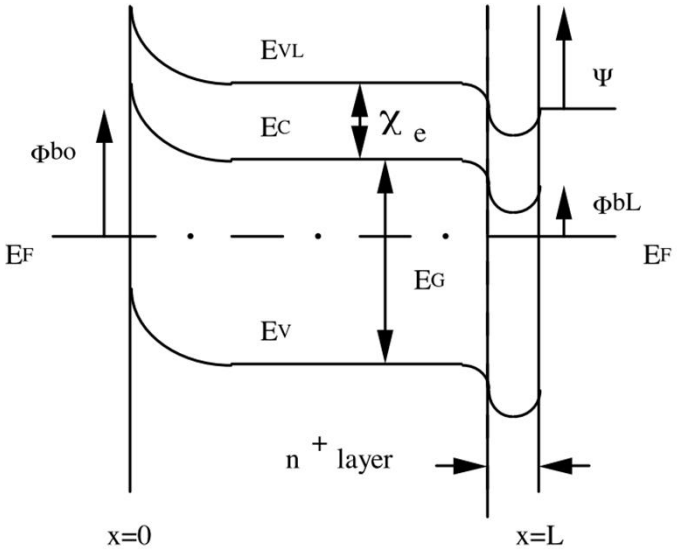

Figure 2-1. A band diagram of a Schottky barrier in thermodynamic equilibrium.

The Delocalized (Band) State Populations n and p

$$n = N_c F_{1/2} \exp\left(\frac{E_F-E_c}{kT}\right)$$

$$p = N_v F_{1/2} \exp\left(\frac{E_V-E_F}{kT}\right)$$

$$N_c = 2\left(\frac{2\pi m_n^{*} kT}{h^2}\right)^{3/2}$$

$$N_V = 2\left(\frac{2\pi m_p^{*} kT}{h^2}\right)^{3/2}$$

$$F_{1/2}(\eta) = \frac{2}{\sqrt{\pi}}\int_0^{\infty} \frac{E^{1/2}\, dE}{1+\exp(E-\eta)}$$

$$\eta_n = \left(\frac{E_F-E_c}{kT}\right)$$

for free electrons and

$$\eta_p = \left(\frac{E_V-E_F}{kT}\right)$$

By: Dr. Jabbari

$$\gamma_n = \frac{F_{1/2}(\eta_n)}{\exp(\eta_n)} \qquad \gamma_p = \frac{F_{1/2}(\eta_p)}{\exp(\eta_p)}$$

$$n = N_C \gamma_n \exp(\eta_n) \qquad p = N_V \gamma_n \exp(\eta_p)$$

Localized (Gap) State Populations N_D^+, N_A^-, n_t, and p_t

2.1.2.1 Doping Levels (N_D^+ and N_A^-)

$$N_D^+ = N_{dD}^+ + N_{bD}^+$$

for the donor-dopant levels and

$$N_A^- = N_{dA}^- + N_{bA}^-$$

for the acceptor-dopant levels.

N_{dD}^+ and N_{dA}^- represent the total charge originating from discrete donor and acceptor concentrations, respectively, while N_{bD}^+ and N_{bA}^- represent the total charge developed by any banded donor and acceptor levels, respectively.

2.1.2.1a Discrete Dopant Levels ($N_{dD,i}$ and $N_{dA,j}$)

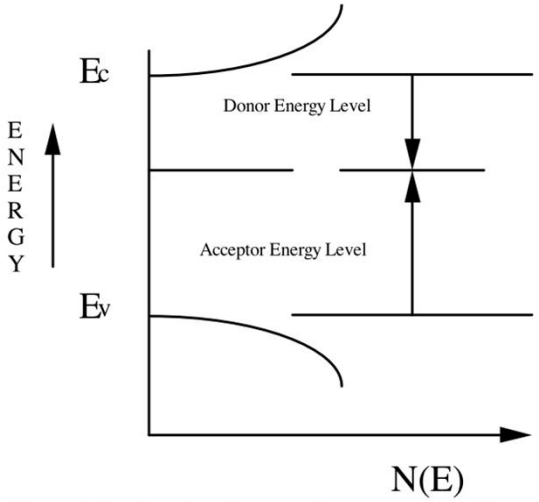

Figure 2-2. Density of states plot representing discrete localized dopant levels. The donor levels are located positively down from the conduction band and the acceptor levels are located positively up from the valence band.

The charge arising from a set of i of these discrete dopant states can be expressed as

$$N_{dD}^{+} = \sum_{i} N_{dD,i}\, \mathbf{f}_{D,i}$$

if they are donor-like and from a set of j of these discrete dopant states as

$$N_{dA}^{-} = \sum_{i} N_{dA,j}\, \mathbf{f}_{A,j}$$

$$\mathbf{f}_{D,i} = \frac{1}{1+\exp\left(\frac{E_F - E_i}{kT}\right)} \qquad \mathbf{f}_{A,j} = \frac{1}{1+\exp\left(\frac{E_j - E_F}{kT}\right)}$$

Using the Shockley-Read-Hall (S-R-H) model

$$\mathbf{f}_{D,i} = \frac{\sigma_{pdD_i} \bullet p + \sigma_{ndD_i} \bullet \gamma_{n_i} \bullet n_{1_i}}{\sigma_{ndD_i}(n+\gamma_{n_i} \bullet n_{1_i}) + \sigma_{pdD_i}(p+\gamma_{p_i} \bullet p_{1_i})} \qquad (2.1.2.1g)$$

The corresponding expression for the jth discrete acceptor-like gap state of energy E_j in the gap is

$$\mathbf{f}_{A,j} = \frac{\sigma_{ndA_j} \bullet n + \sigma_{pdA_j} \bullet \gamma_{p_j} \bullet p_{1_j}}{\sigma_{ndA_j}(n+\gamma_{n_j} \bullet n_{1_j}) + \sigma_{ndA_j}(p+\gamma_{p_j} \bullet p_{1_j})} \qquad (2.1.2.1h)$$

In these expressions $\sigma_{ndD_i}(E_i)$ and $\sigma_{pdD_i}(E_i)$ are the capture cross sections for electrons and holes of the ith donor-like discrete levels, respectively. $\sigma_{ndA_j}(E_j)$ and $\sigma_{pdA_j}(E_j)$ are the capture cross section for electrons and holes at the jth acceptor site, and $n_{1_k}(E_k)$ and $p_{1_k}(E_k)$ are parameters that can be expressed as

$$n_{1_k}(E_k) = N_c \exp\left(\frac{E_k - E_c}{kT}\right) \qquad (2.1.2.1i)$$

$$p_{1_k}(E_k) = N_v \exp\left(\frac{E_v - E_k}{kT}\right) \qquad (2.1.2.1j)$$

2.2 The Continuity Equations

$$\frac{1}{q}\left(\frac{dJ_n}{dx}\right) = -G_{op}(x) + R(x)$$

$$\frac{1}{q}\left(\frac{dJ_p}{dx}\right) = G_{op}(x) - R(x)$$

$$J_n(x) = q\mu_n n\left(\frac{dEf_n}{dx}\right)$$

$$R(x) = R_D(x) + R_I(x)$$

$$\hat{R}_D(x) = R - G_{th} = \beta(np - \hat{n}_o\hat{p}_o) = \beta(np - n_i^2)$$

$$J_p(x) = q\mu_p p\left(\frac{dEf_p}{dx}\right)$$

$$R_I(x) = (np - n_i^2)$$

2.2.2.2 Indirect (Shockley-Read-Hall) Recombination

$$\left\{ \sum_i \left[\frac{N_{dD_i}\sigma_{ndD_i}\sigma_{pdD_i}\nu_{th}}{\sigma_{ndD_i}(n+n_1(E_i))+\sigma_{pdD_i}(p+p_1(E_i))} + \frac{N_{bD_i}}{W_{Di}} \int_{E_{1i}}^{E_{2i}} \frac{\sigma_{nbD_i}\sigma_{pbD_i}\nu_{th}dE}{\sigma_{nbD_i}(n+n_1(E))+\sigma_{pbD_i}(p+p_1(E))} \right] \right.$$

$$+ \sum_j \left[\frac{N_{dA_j}\sigma_{ndA_j}\sigma_{pdA_j}\nu_{th}}{\sigma_{ndA_j}(n+n_1(E_j))+\sigma_{pdA_j}(p+p_1(E_j))} + \frac{N_{bA_j}}{W_{Aj}} \int_{E_{1j}}^{E_{2j}} \frac{\sigma_{nbA_j}\sigma_{pbA_j}\nu_{th}dE}{\sigma_{nbA_j}(n+n_1(E))+\sigma_{pbA_j}(p+p_j(E))} \right]$$

$$+ \sum_i \left[\frac{n_{dD_{t_i}}\sigma_{ndD_i}\sigma_{pdD_i}\nu_{th}}{\sigma_{ndD_i}(n+n_1(E_i))+\sigma_{pdD_i}(p+p_1(E_i))} + \frac{n_{bD_{t_i}}}{W_{Dt_i}} \int_{E_{1i}}^{E_{2i}} \frac{\sigma_{nbD_i}\sigma_{pbD_i}\nu_{th}dE}{\sigma_{nbD_i}(n+n_1(E))+\sigma_{pbD_i}(p+p_1(E))} \right]$$

$$+ \sum_j \left[\frac{n_{dA_{t_j}}\sigma_{ndA_j}\sigma_{pdA_j}\nu_{th}}{\sigma_{ndA_j}(n+n_1(E_j))+\sigma_{pdA_j}(p+p_1(E_j))} + \frac{n_{bA_{t_j}}}{W_{At_j}} \int_{E_{1j}}^{E_{2j}} \frac{\sigma_{nbA_j}\sigma_{pbA_j}\nu_{th}dE}{\sigma_{nbA_j}(n+n_1(E))+\sigma_{pbA_j}(p+p_1(E))} \right]$$

$$\left. + \int_{E_v}^{E_c} \frac{g_D(E)\sigma_{nc_D}\sigma_{pc_D}\nu_{th}\,dE}{\sigma_{nc_D}(n+n_1(E))+\sigma_{pc_D}(p+p_1(E))} + \int_{E_v}^{E_c} \frac{g_A(E)\sigma_{nc_A}\sigma_{pc_A}\nu_{th}\,dE}{\sigma_{nc_A}(n+n_1(E))+\sigma_{pc_A}(p+p_1(E))} \right\} \quad (2.2.2.2a)$$

2.2.3 Optical Generation Rate

$$G_{op}(x) = \frac{-d}{dx}\sum_i \Phi_i^{FOR}(\nu_i) + \frac{d}{dx}\sum_i \Phi_i^{REV}(\nu_i)$$

where $\Phi_i^{FOR}(\nu_i)$ represents the photon flux of frequency ν_i at some point x which is moving left to right in Fig 2-5 and $\Phi_i^{REV}(\nu_i)$ represents the photon flux of frequency ν_i at some point x which is moving right to left in Fig 2-5.

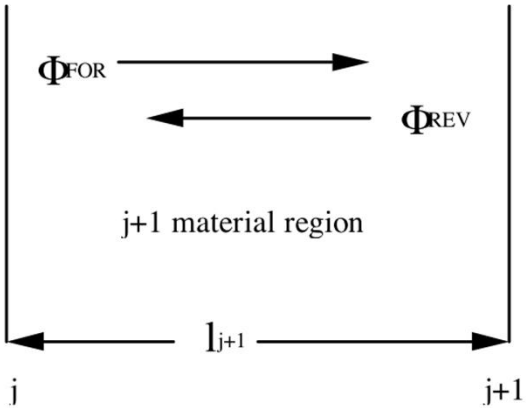

Figure 2-5. This figure illustrates the photon flux at some point x moving to the left and the photon flux at some point x moving to the right in the j+1 material region.[1]

If a device has optical properties that do not vary across the structure then, at some general point x, we have

$$\Phi_i^{FOR}(\nu_i) = \Phi_{oi}(\nu_i)\bullet\{\exp[-\alpha(\nu_i)x] + R_F R_B[\exp(-\alpha(\nu_i)L)]^2 \bullet \exp[-\alpha(\nu_i)x] + \ldots\} \qquad (2.2.3b)$$

$$\Phi_i^{REV}(\nu_i) = R_B\Phi_{oi}(\nu_i)\bullet\{\exp[-\alpha(\nu_i)L]\bullet\exp[-\alpha(\nu_i)(L-x)] + R_F R_B[\exp(-\alpha(\nu_i)L)]^3 \bullet \exp[-\alpha(\nu_i)(L-x)] + \ldots\}$$

In these expressions R_F is the reflection coefficient for the internal surface at x=0 and R_B is the reflection coefficient for the internal surface at x=L (the back surface). All of these reflection coefficients can be functions of the frequency ν_i. Any reflection and loss that may occur before x=0 (such as that at any air/glass and that in any transparent conductive oxide layer) must be accounted fro a priori by the user appropriately adjusting $\Phi_{oi}(\nu_i)$.

The reflection coefficient R_j at the j - boundary

$$R_j = \left\{ \frac{\left[\left(\frac{\varepsilon_{j-1}}{\varepsilon_j} \right)^{1/2} - 1 \right]}{\left[\left(\frac{\varepsilon_{j-1}}{\varepsilon_j} \right)^{1/2} + 1 \right]} \right\}^2 \qquad R_{j+1} = \left\{ \frac{\left[\left(\frac{\varepsilon_{j+1}}{\varepsilon_j} \right)^{1/2} - 1 \right]}{\left[\left(\frac{\varepsilon_{j+1}}{\varepsilon_j} \right)^{1/2} + 1 \right]} \right\}^2$$

As outlined in Appendix A, the result for the j+1 material layer is

$$\Phi_i^{FOR}(\nu_i) = \Phi_j^{LR}\{1 + R_j R_{j+1}[\exp(-\alpha_{j+1} l_{j+1})]^2 + \dots\}\exp[-\alpha_{j+1}(x-x_j)]$$
$$+ R_j \Phi_{j+1}^{RL}\{\exp(-\alpha_{j+1} l_{j+1}) + R_j R_{j+1}[\exp(-\alpha_{j+1} l_{j+1})]^3 + \dots\}\exp[-\alpha_{j+1}(x-x_j)]$$

Similarly, for the j+1 material layer

$$\Phi_i^{REV}(\nu_i) = \Phi_{j+1}^{RL}\{1 + R_j R_{j+1}[\exp(-\alpha_{j+1} l_{j+1})]^2 + \dots\}\exp[-\alpha_{j+1}(x_{j+1}-x)]$$
$$+ R_{j+1} \Phi_j^{LR}\{\exp(-\alpha_{j+1} l_{j+1}) + R_j R_{j+1}[\exp(-\alpha_{j+1} l_{j+1})]^3 + \dots\}\exp[-\alpha_{j+1}(x_{j+1}-x)]$$

2.2.4 Boundary Conditions

$$\Psi(0) = \Psi_o - V$$

$$\Psi(L) = 0$$

$$J_p(0) = -qS_{po}(p_o(0) - p(0))$$

$$J_p(L) = qS_{pL}(p(L) - p_o(L))$$

$$J_n(0) = qS_{no}(n(0) - n_o(0))$$

$$J_n(L) = -qS_{nL}(n_o(L) - n(L))$$

2.3 Solution Techniques

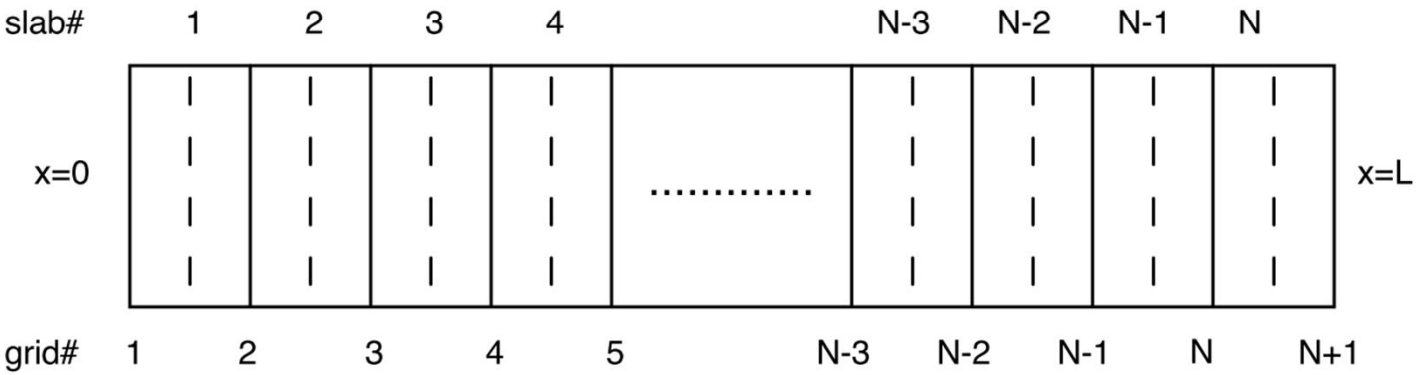

Figure 2-7. A grid used in numerical methods. There are N slabs (dashed lines) and N+1 major grid points (solid lines). The example shown here is a uniform grid.

Poisson's equation is represented by finite central differences

$$\frac{d^2\Psi(x_i)}{dx^2} = \frac{\Psi x_{i+1} - 2\Psi x_i + \Psi x_{i-1}}{h+H}$$

$$\left[\frac{dJ_p}{dx}\right]_i = \frac{J_{p_{i+1/2}} - J_{p_{i-1/2}}}{h+H}$$

for the hole continuity equation and

$$\left[\frac{dJ_n}{dx}\right]_i = \frac{J_{n_{i+1/2}} + J_{n_{i-1/2}}}{h+H}$$

$$J_{p,i+\frac{1}{2}} = -q\mu_p p_i\left(\frac{dE_{f_p}}{dx}\right) = -q\mu_p N_v \exp\left(\frac{\Phi_{b_L} - E_G + E_{f_p} + \Psi}{kT}\right)\left(\frac{dE_{f_p}}{dx}\right)$$

$$J_{p,i+\frac{1}{2}} \exp(-\Psi/kT)dx = -q\mu_p N_v \exp\left(\frac{\Phi_{b_L} - E_G + E_{f_p}}{kT}\right)de_{f_p}$$

$$\Psi(x) = \left[\frac{\Psi_{i+1} - \Psi_i}{H}\right](x - x_i) + \Psi_i$$

$$\int_i^{i+1} q\mu_p N_v \exp\left(\frac{\Phi_{b_L} - E_G + E_{f_p}}{kT}\right)\bullet dE_{f_p} = \left[q\mu_p N_v \exp\left(\frac{\Phi_{b_L} - E_G + E_{f_p}}{kT}\right)\bullet kT\right]_i^{i+1}$$

evaluated from i to i+1

$$q\mu_p N_v kT \exp\left(\frac{\Phi_{b_L} - E_{G_i}}{kT}\right)\left[\exp\left(\frac{E_{f_{pi+1}}}{kT}\right) - \exp\left(\frac{E_{f_{pi}}}{kT}\right)\right]$$

$$J_{p,i+\frac{1}{2}} = \frac{\left[\frac{qkT\mu_p N_v \exp\left(\frac{-\phi_{bL} - E_G}{kT}\right)}{H}\right]\left[\exp\left(\frac{E_{fp_{i+1}}}{kT}\right) - \exp\left(\frac{E_{fp_i}}{kT}\right)\right]\left[\frac{\Psi_{i+1}}{kT} - \frac{\Psi_i}{kT}\right]}{\left[\exp\left(\frac{-\Psi_{i+1}}{kT}\right) - \exp\left(\frac{-\Psi_i}{kT}\right)\right]} \qquad \text{(B-9)}$$

Using the same approach as above, the corresponding expression for the electron current density is

$$J_{n,i+\frac{1}{2}} = \frac{\left[\frac{qkT\mu_n N_c \exp\left(\frac{-\phi_{bL}}{kT}\right)}{H}\right]\left[\exp\left(\frac{E_{fn_{i+1}}}{kT}\right) - \exp\left(\frac{E_{fn_i}}{kT}\right)\right]\left[\frac{\Psi_{i+1}}{kT} - \frac{\Psi_i}{kT}\right]}{\left[\exp\left(\frac{\Psi_{i+1}}{kT}\right) - \exp\left(\frac{\Psi_i}{kT}\right)\right]} \qquad \text{(B-10)}$$

$$\left[\frac{dJ_p}{dx}\right]_i = \frac{J_{p_{i+1/2}} - J_{p_{i-1/2}}}{H+h}$$

and

$$\left[\frac{dJ_n}{dx}\right]_i = \frac{J_{n_{i+1/2}} - J_{n_{i-1/2}}}{H+h}$$

With this discretization of the derivatives in Poisson's equation and in the two continuity equations, these equations may be recast as three functions f_i, f_{e_i}, and f_{h_i} and expressed in difference form. The equation for f_i, which corresponds to Poisson's equation, is

$$f_i(\Psi^*_{i-1},\Psi^*_i,\Psi^*_{i+1}) = -(A^*_{i-1}\Psi^*_{i-1} - A^*_i\Psi^*_i + A^*_{i+1}\Psi^*_{i+1}) + \rho_i(\Psi^*_i) \qquad (2.3.2d)$$

$$\Psi^* = \Psi/kT.$$

$$A^*_{i-1} = \frac{4\varepsilon_i\varepsilon_{i-1}kT}{h(h+H)(\varepsilon_i+\varepsilon_{i-1})}, \qquad A^*_i = kT*A_i.$$

$$A^*_{i+1} = \frac{4\varepsilon_i\varepsilon_{i+1}kT}{H(h+H)(\varepsilon_i+\varepsilon_{i+1})},$$

and

$$A^*_i = A^*_{i-1} + A^*_{i+1}$$

$$f_{e_i}(x) = \frac{2}{q(h+H)}[J_{n,i+1/2}(x) - J_{n,i-1/2}(x)] + G_{op,i}(x) - R_i(x)$$

$$f_{h_i}(x) = -\frac{2}{q(h+H)}[J_{p,i+1/2}(x) - J_{p,i-1/2}(x)] + G_{op,i}(x) - R_i(x)$$

2.3.3 Newton-Raphson Method

The Newton-Raphson Method is used in AMPS to solve this set of 3(N+1) algebraic equations resulting from breaking a device structure into N slabs and from writing the governing differential equations in terms of differences in the state variables Ψ, E_{Fn} and E_{Fp} at the grid points defining these slabs. It is a method that iteratively finds the roots of a set of functions f_i, f_{e_i}, and f_{h_i}, if given an adequate initial guess for the roots. We stress that the key to success (convergence) is having an adequate initial guess. Routines are built into AMPS to generate these initial guesses.

$$[A]\bullet[\delta] = [B]$$

The matrix δ is constructed as

$$\begin{bmatrix} \Uparrow \\ \delta\ \Psi \\ \delta\ E_{fp_i} \\ \delta\ E_{fn_i} \\ \Downarrow \end{bmatrix}$$

and the matrix B is constructed as

$$\begin{bmatrix} \Uparrow \\ f_i \\ f_{e_i} \\ f_{h_i} \\ \Downarrow \end{bmatrix}$$